JOC The Journal of Organic Chemistry

Article

pubs.acs.org/joc

Synthesis of Methoxy-Substituted Picenes: Substitution Position Effect on Their Electronic and Single-Crystal Structures

Hiroki Mori,[†] Xi-chao Chen,[†] Ning-hui Chang,[†] Shino Hamao,[‡] Yoshihiro Kubozono,[‡,§] Kiyohiko Nakajima,[∥] and Yasushi Nishihara*[,†,§]

[†]Division of Earth, Life, and Molecular Sciences, Graduate School of Natural Science and Technology, Okayama University, 3-1-1 Tsushimanaka, Kita-ku, Okayama 700-8530, Japan

[‡]Research Laboratory for Surface Science, Okayama University, 3-1-1 Tsushimanaka, Kita-ku, Okayama 700-8530, Japan

[§]ACT-C, Japan Science and Technology Agency, 4-1-8 Honcho, Kawaguchi, Saitama 332-0012, Japan

[∥]Department of Chemistry, Aichi University of Education, 1 Hirosawa, Igaya-cho, Kariya, Aichi 448-8542, Japan

Supporting Information

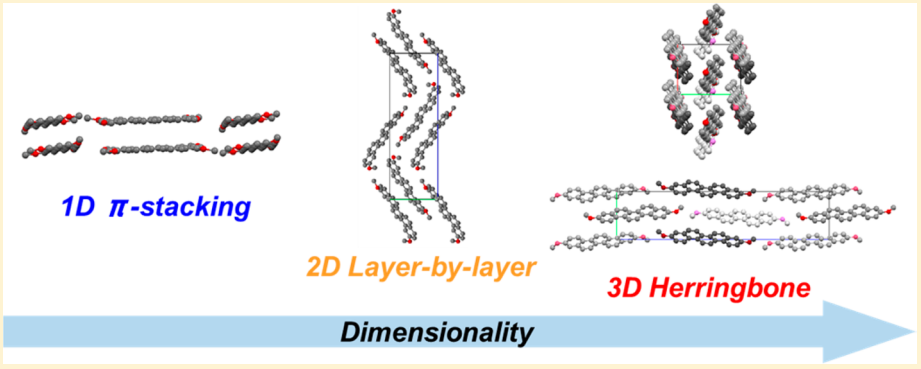

ABSTRACT: A series of picenes having methoxy groups was synthesized through Pd-catalyzed Suzuki−Miyaura couplings or Wittig reaction/intramolecular cyclization sequences, and their physicochemical properties and single-crystal structures were evaluated. The substitution position effects between the outer 1,12-, 2,11-, and 4,9-position and the inner 3,10-position are quite different; the former showed the same electronic structure as that of picene, but the latter results in a HOMO geometry different from those of picene and other methoxy picenes. In addition, crystal structures of four types of methoxy-substituted picenes **4a−c,e** strongly depend on their substitution position and number of methoxy groups, which dramatically changes the structures from the fully anisotropic 1D π-stacked structure to a unique 3D herringbone structure due to steric hindrance of methoxy groups. The calculations of transfer integrals based on their single-crystal structures reveal that the methoxy picenes have intermolecular overlaps less effective than that of the parent nonsubstituted picene. These results are attributed not only to the packing structure but also to electronic structures such as the HOMO distribution. The preliminary OFET of the representative **4c,e** showed hole mobilities significantly lower than that of picene due to their less effective intermolecular overlaps, as predicted by the calculated transfer integrals.

INTRODUCTION

Aromatic compounds with extended π conjugation have attracted significant interest because of their high potential for use in organic electronic devices such as organic field-effect transistors (OFETs), light-emitting diodes (OLEDs), and photovoltaic cells (OPVs).[1] Among them, a linearly fused system, such as pentacene and its derivatives, has been intensively applied to organic materials for electronic devices.[2] However, pentacene is quite unstable on exposure to light and air due to its relatively high HOMO energy level (−5.0 eV) originating from its highly π-conjugated nature, which limits its practical application in electronic devices.[3] On the other hand, picene, an isostructural analogue of pentacene, is known to be a stable compound (E_{HOMO} = −5.8 eV), in which the benzene rings are fused in an armchair structure. It represents a novel and promising class of materials for organic electronics. An FET device with a thin film of picene showed a high mobility (μ) value of more than 5 $cm^2\ V^{-1}\ s^{-1}$, and its FET properties are known to be improved with the μ value as well as the on−off ratio under air or O_2.[4] Additionally, picene can be used in superconductors: a picene doped with an alkali metal such as potassium or rubidium exhibited superconductivity below 18 K.[5]

To further utilize picene for organic semiconducting materials, an efficient method of synthesizing functionalized

Received: March 7, 2014
Published: May 2, 2014

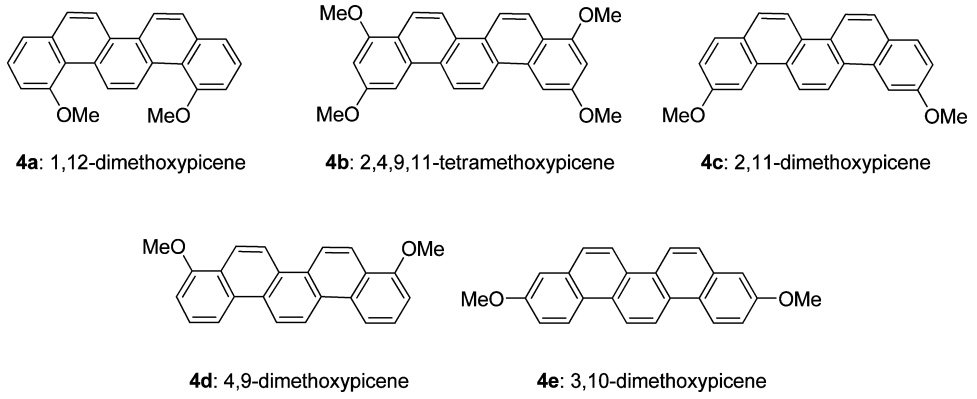

Figure 1. Structures of methoxy picenes **4a–e** in this study.

Scheme 1. Synthesis of 4a–d by Suzuki–Miyaura Coupling/Intramolecular Cyclization Sequences

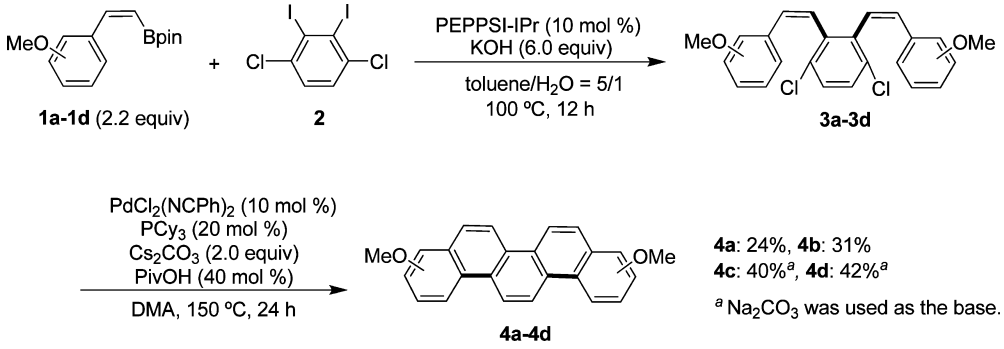

Scheme 2. Synthesis of 4e via Wittig Reaction

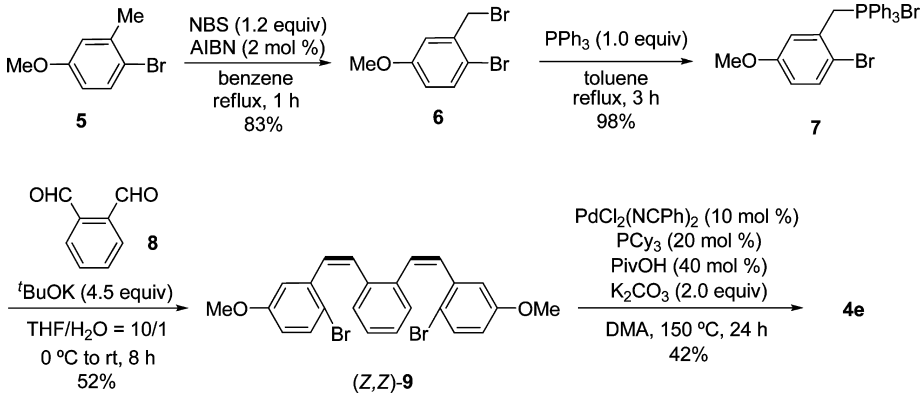

picene is highly desirable for the following reasons. First, the introduction of solubilizing groups on the picene core would allow the development of soluble picene-based materials suitable for the solution process, while nonsubstituted picene generally has poor solubility. Second, the introduction of substituents can alter a perturbation on the basis of the electronic structures of the core, resulting in different HOMO and LUMO energy levels, which are very important for electronic devices. Third, the kind, the position, and the number of substituents significantly affect the packing structure in the solid state, which is critical for efficient carrier transport. Thus, many researchers have succeeded in developing efficient methods of synthesizing parent and functionalized picenes.[6] However, there are still several drawbacks to these methods, such as a tedious series of multiple steps needed for their preparation, the use of expensive reagents and catalysts, and the limitations of the substrates. Furthermore, there is no example of highly selective synthesis of various isomeric picenes, and hence a systematic comparison of electronic structures and solid-state properties in a series of substituted picenes has not been investigated. Very recently, we have reported a new method for the synthesis of substituted picenes through the palladium-catalyzed Suzuki–Miyaura cross-coupling of stereodefined (*Z*)-alkenylboronates with polyhalobenzene and sequential intramolecular double cyclization via direct C–H bond activation.[7] In order to analyze the systematic trends of physical properties of the isomeric picenes, we herein report the synthesis of five kinds of methoxy-substituted picenes in different substitution positions (Figure 1), their physicochemical properties and intermolecular transfer integrals (*ts*) based on their single crystal X-ray analyses, and FET mobilities of several representative methoxy picenes.

dx.doi.org/10.1021/jo500543h | J. Org. Chem. 2014, 79, 4973–4983

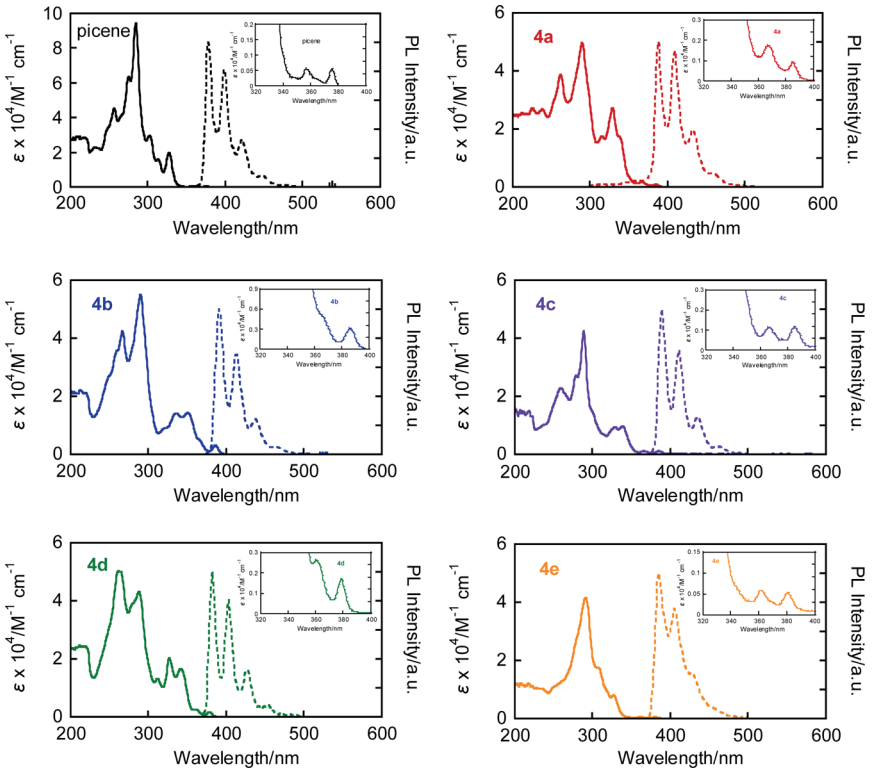

Figure 2. Absorption spectra (1×10^{-5} M) and fluorescence spectra with excitation wavelength at λ_{max}^{abs} (1×10^{-6} M) of **4a–e** in CH_2Cl_2.

RESULTS AND DISCUSSION

Synthesis of 4a–d by Suzuki–Miyaura Coupling/Intramolecular Cyclization Sequences. With our previously reported method of synthesizing substituted picenes for reference,[7] we investigated the Suzuki–Miyaura coupling of stereodefined (*Z*)-alkenylboronates **1a–d** bearing methoxy groups with 1,4-dichloro-2,3-diiodobenzene (**2**) to generate **3a–d**, which were further subjected to Pd-catalyzed intramolecular double cyclization via C–H activation,[8,9] affording the corresponding di- and tetramethoxy picenes **4a–d** in 24–42% yields (Scheme 1). The origin of relatively low yields of the desired products can be attributed to the occurrence of isomerizarion that leads to the formation of *E* isomers of **3a–d** during Suzuki–Miyaura coupling and/or protodechlorination over the course of the subsequent double cyclization.

Synthesis of 4e by Wittig Reaction/Intramolecular Cyclization Sequences. Since the aforementioned method of synthesis selectively gave rise to the formation of **4a** through intramolecular double cyclization, we synthesized 3,10-dimethoxypicene (**4e**) using a different strategy. In this new method shown in Scheme 2, the precursor **9** has only one reaction site, which enabled the selective synthesis of **4e** after the Pd-catalyzed intramolecular double cyclization. First, (2-bromo-5-methoxybenzyl)triphenylphosphonium bromide (**7**), derived from commercially available **5**, reacted with phthalic dialdehyde (**8**) to give the precursor (*Z*,*Z*)-**9** in 52% yield.[10] After the optimization of the conditions shown in Table S1 (Supporting Information), the subsequent Pd-catalyzed intramolecular cyclization afforded the desired product **4e** in 42% yield.

UV–Vis Absorption and Fluorescence Spectra of 4a–e. UV–vis absorption spectra of methoxy picenes **4a–e** are shown in Figure 2, and their optical properties are summarized in Table 1 and compared with those of picene. The absorption

Table 1. UV–Vis[a] and Fluorescence[b] Data of 4a–e

compd	λ_{max}^{abs}, nm	ε, M^{-1} cm^{-1}	E_g^{opt}, eV[c]/ λ_{edge}, nm	λ_{max}^{em}, nm[d]	Stokes shift, cm^{-1}
picene[e]	285	94300	3.23/384	378	212
4a[e]	290	49700	3.13/396	388	201
4b[e]	290	55100	3.08/402	391	331
4c	289	42500	3.13/396	389	267
4d	262, 288	50200, 43100	3.14/395	382	242
4e	291	41500	3.15/393	385	273

[a] 1×10^{-5} M in CH_2Cl_2. [b] 1×10^{-6} M in CH_2Cl_2. [c] Estimated with the absorption edge (λ_{edge}). [d] Wavelength of fluorescence maximum. [e] Our previous work.[7]

maxima (λ_{max}^{abs}) of **4a–e** were slightly red shifted in comparison to that of picene. Among them, **4a**,**b**,**d** have a relatively intense absorption at around 270 nm in comparison to that of picene. In particular, this transition of **4d** is the most intense and has a λ_{max} value of 262 nm, which indicates that the introduction of methoxy groups to the 1,12- and 4,9-positions may enhance their transition. Methoxy picenes **4a–d** exhibited red-shifted absorption bands at around 360–380 nm, corresponding to an $S_0 \rightarrow S_1$ transition.[11] In addition, new and more intense absorption peaks around 340–380 nm derived from an $S_0 \rightarrow S_1$ transition may reflect the difference in their electronic structures. HOMO–LUMO energy gaps (E_g) estimated from their absorption edges are 3.13 eV for **4a**,**c**, 3.08 eV for **4b**, and 3.14 eV for **4d**, which are smaller than that of picene. These results suggest that the strong electron-donating nature of methoxy groups directly affects the electronic structures of the picene core, resulting in red-shifted absorption bands, intense absorption peaks, and smaller energy gaps. In sharp contrast, the absorption spectrum of **4e** also showed a red-shifted absorption band around 360–380 nm, but the

dx.doi.org/10.1021/jo500543h | J. Org. Chem. 2014, 79, 4973–4983

spectral shape did not change dramatically in comparison to that of picene, though **4e** also has two strong electron-donating methoxy groups. In particular, no absorption peak was observed around 340−360 nm in **4e**, suggesting that the substitution effect of 3,10-positions is small, as evidenced from our previous work,[7] or that **4e** may have a different electronic structure in comparison to that of picene and the four other methoxy picenes **4a**−**d**.

The fluorescence spectra of **4a**−**e** have nearly identical features and exhibited a vibronic structure that is similar to that of picene. The emission maxima (λ_{max}^{em}) were bathochromically shifted from that of the parent picene, but the substitution position effect on their fluorescence spectra is rather small. Stokes shifts of methoxy picenes, except for **4a**, increased with an increasing number of methoxy groups, indicating that the introduction of methoxy groups onto the 2,3,4,9,10,11-positions leads to large structural changes between the ground and excited states. However, **4a** has a smaller Stokes shift than that of picene, implying that **4a** has a rigid and coplanar structure due to the introduction of methoxy groups onto the 1,12-positions in the excited state.

Electrochemical Properties of 4a−e. Next, the electrochemical properties of methoxy picenes **4a**−**e** were investigated by cyclic voltammetry. Figure 3 shows the cyclic voltammo-

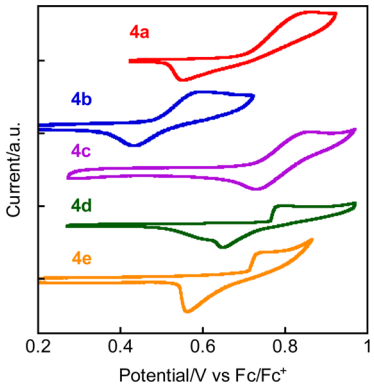

Figure 3. Cyclic voltammograms of **4a**−**e** in CH_2Cl_2 solution containing 0.1 M Bu_4NPF_6 as supporting electrolyte at a scan rate of 100 mV s^{-1}.

grams of **4a**−**e**, and their electrochemical data are summarized in Table 2. Cyclic voltammograms of the five methoxy picenes **4a**−**e** showed one oxidation wave with a clear reduction process, and they showed oxidation onsets at +0.49−0.73 V (vs Fc/Fc^+). In comparison with the parent picene, their HOMO energy levels, determined to be 5.29−5.56 eV below the vacuum level from the onset of the oxidation peaks, were

Table 2. Electrochemical Data of 4a−e

compd	E_{onset}, V[a]	E_{HOMO}, eV[b]	E_{LUMO}, eV[c]
picene[d]	+1.00	−5.80	−2.57
4a[d]	+0.71	−5.51	−2.38
4b[d]	+0.49	−5.29	−2.21
4c	+0.73	−5.53	−2.40
4d	+0.76	−5.56	−2.42
4e	+0.71	−5.51	−2.36

[a]Oxidation onset vs Fc/Fc^+. [b]Estimated with the equation E_{HOMO} (eV) = −4.8 − $E_{1/2}$ − E_{onset}. [c]Calculated according to the formula $E_{LUMO} = E_{HOMO} + E_g^{opt}$. [d]Our previous work.[7]

elevated significantly as the number of methoxy groups increased. In these cases, methoxy groups introduced onto the picene framework in any position simply act as the strong electron-donating group, even in **4e**. Actually, as UV−vis results suggested, the electronic structure of **4e** may be different from those of picene and the four other methoxy picenes **4a**−**d**, although the HOMO energy level of **4e** also increases in the same manner as for **4a**−**d** by methoxy substituents. The elevation of HOMO energy levels found in the five methoxy picenes **4a**−**e** may contribute to a lowering of the contact resistance between the gold source electrodes and active layers (**4a**−**e**) in OFET devices.

Theoretical Calculations of HOMO and LUMO in 4a−e. To investigate the electronic structures of methoxy picenes **4a**−**e** in detail, theoretical calculations of their HOMO and LUMO were carried out with density functional theory (DFT) at the B3LYP/6-31G(d) level using Gaussian 09, Revision A.02.[12] Figure 4 shows the molecular orbitals and calculated energy diagrams of **4a**−**e**. In **4a**,**b**,**d**, the geometries of both the HOMO and LUMO are quite similar to those of picene: the coefficient of the HOMO in these methoxy picenes was delocalized not only over the entire molecular π framework but also onto the oxygen atoms of the terminal methoxy groups. Reflecting this feature, HOMO levels of **4a**,**b**,**d** were elevated significantly as the number of methoxy substituents increased. In addition, their HOMO−LUMO energy gaps become small, which is consistent with the results of their absorption spectra. These results can be understood if it is considered that the introduction of methoxy groups onto the 1,12-, 4,9-, and 2,4,9,11-positions directly affects the frontier orbitals of the picene core. The geometry of HOMO in **4c** is also similar to those of picene and **4a**,**b**,**d**, but a small difference was observed. The geometry of the LUMO and LUMO+1 in **4c** is reversed with respect to picene (Figure S1, Supporting Information); the energy difference between the LUMO (−1.08 eV) and LUMO +1 (−1.05 eV) in **4c** is quite small. This result suggests that the substitution in the 2,11-positions has the effect of stabilizing the LUMO. In fact, although **4b** with methoxy groups in the 2,11-positions does not have an inverted LUMO and LUMO+1, the energy difference between the LUMO and LUMO+1 in **4b** is also quite small (LUMO = −0.83 eV, LUMO+1 = −0.84 eV). For this reason, a small difference in the absorption spectra among **4a**,**c**,**d** bearing two methoxy groups could be observed. However, the obtained actual energy gaps of **4a**,**c**,**d** were almost identical, which suggests that the electronic structure of **4c** is similar to that of **4a**,**d**.

In contrast, the HOMO of **4e** is quite different from that of picene, though the geometry of the LUMO is the same. This feature is different from what we found in our previous work in the case of 3,10-trimethylsilyl picene.[7] Interestingly, the HOMO and HOMO-1 in **4e** are reversed with respect to that of picene (Figure S1, Supporting Information). The HOMO and HOMO-1 energy levels of **4e** are −5.24 and −5.38 eV, respectively, which suggests that methoxy groups in the 3,10-positions stabilize the HOMO energy level, whereas the HOMO-1 energy level becomes very unstable. Thus, the small substitution effect on absorption spectra between picene and **4e** had a significant effect on their intrinsically different electronic structures. This change in HOMO distribution may affect their intermolecular overlaps: i.e., intermolecular transfer integrals of HOMO in the solid state.[13]

From LUMO orbitals of all methoxy picenes **4a**−**e**, coefficients of the LUMO were also slightly delocalized onto

dx.doi.org/10.1021/jo500543h | J. Org. Chem. 2014, 79, 4973−4983

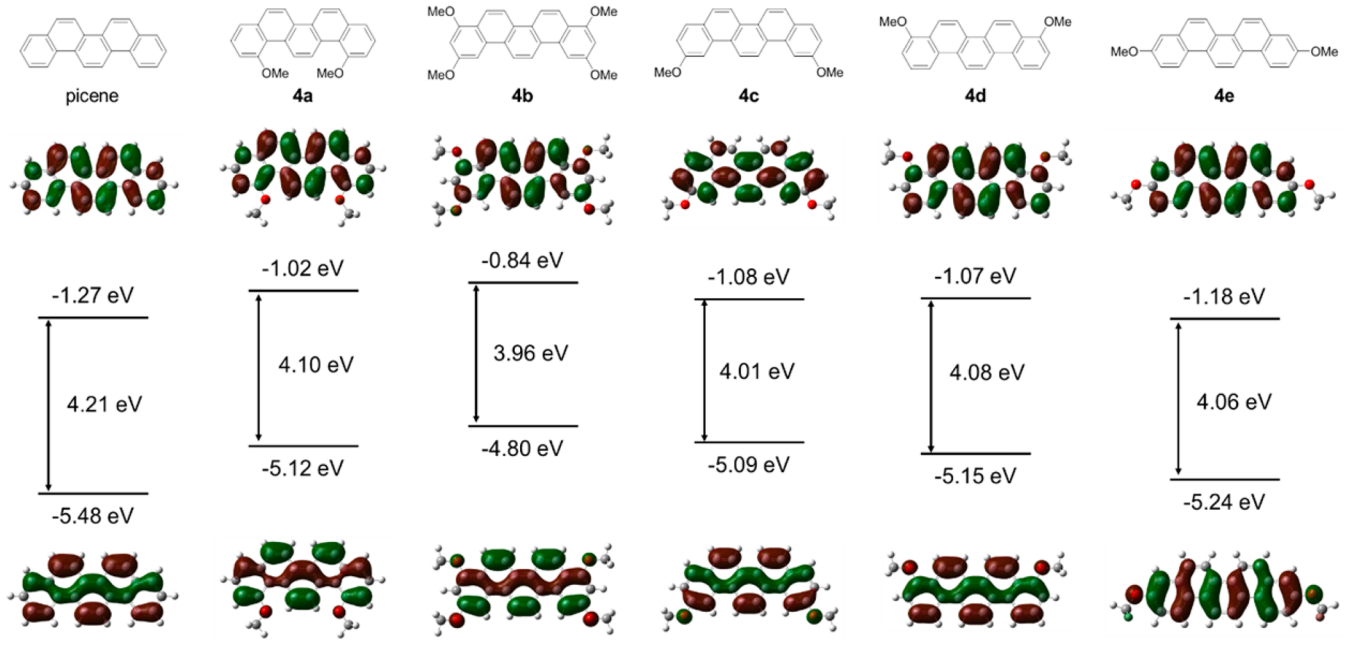

Figure 4. Calculated HOMOs and LUMOs of picene and **4a**–**e** at the DFT B3LYP/6-31(d) level.

the oxygen atoms, but their contributions were rather smaller than those of HOMO. This result suggests that the substitution effect of methoxy groups on LUMO levels (destabilization of the LUMO by the methoxy groups) is small, resulting in a HOMO–LUMO energy gap smaller than that of picene.

To further investigate the application of these methoxy picenes to semiconducting materials, we calculated the molecular reorganization energies of holes (λ_hs), which may potentially affect the hole-transporting ability.[14] The calculated λ_hs are 185 meV for picene, 168 meV for **4a**, 277 meV for **4b**, 244 meV for **4c**, 220 meV for **4d**, and 260 meV for **4e**. In general, alkoxy substituents in the core tend to show λ values larger than that of the parent core because large geometrical changes in the alkoxy-substituted materials occur upon oxidation.[15] However, to our surprise, **4a** has a λ value smaller than that of picene. In order to understand these differences, we investigated the geometrical changes upon oxidation in the parent picene and methoxy picenes **4a**–**e**. Their calculated bond length changes between the optimized neutral and cationic states are summarized in Table S2 (Supporting Information). Among picenes **4a**,**c**–**e** having two methoxy groups, the largest C–C bond length changes are almost the same (0.020–0.023 Å), but significant geometrical changes in the C–O bonds are observed in **4c**–**e**; the C–O bond lengths decreased by 0.026 Å for **4c**, 0.024 Å for **4d**, and 0.030 Å for **4e** upon oxidation. These large geometrical changes may be attributed to their quinoidal species in the cationic state, as evidenced from their optimized structure. In particular, the *p*-anisole-like structure of **4e** may readily form a quinoidal structure upon oxidation, resulting in the largest geometrical change in the C–O bonds and thus the largest λ value among dimethoxy picenes.[16] Whereas geometrical changes in the C–O bonds in **4a** are also observed, the change is relatively small (−0.016 Å). From the optimized structure of **4a** in both the neutral and cationic states, oxygen atoms of **4a** could possibly form hydrogen bonds with the neighboring hydrogen atoms (i.e., the hydrogen atoms on a central benzene ring of picene; calculated distance 2.01 Å), leading to a more planar and rigid backbone. This is the reason **4a** has a λ value smaller than that of picene. These calculations have led us to conclude that only **4a** can be a good candidate as an effective hole-transporting material, but **4a** was found to show a small transfer integral (t) in its crystal structure, as described below.

Single-Crystal Structure Analyses and Transfer Integrals of HOMO in 4a–c,e. As shown in Figure 5, X-ray diffraction analyses unambiguously clarified the structures of dimethoxypicenes **4a**,[7] **4c**, and **4e** and tetramethoxypicene **4b**.[17] The calculations of intermolecular transfer integrals (ts) between the HOMOs in these single crystals were also carried out with the PW91 functional and Slater-type triple-ζ

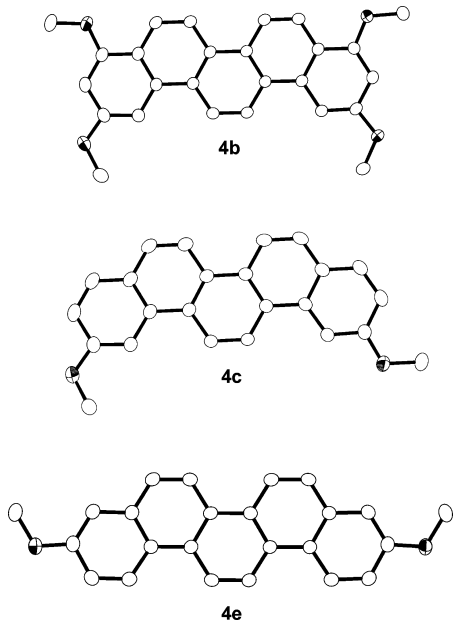

Figure 5. ORTEP drawings of **4b**,**c**,**e** determined by X-ray crystallography with 30% probability thermal ellipsoids. Hydrogen atoms are omitted for simplicity.

dx.doi.org/10.1021/jo500543h | J. Org. Chem. 2014, 79, 4973–4983

polarization (TZP) basis sets using the Amsterdam Density Functional (ADF) package (Figure 6).[18] These calculation results enabled us to predict their hole-transporting characteristics.[19]

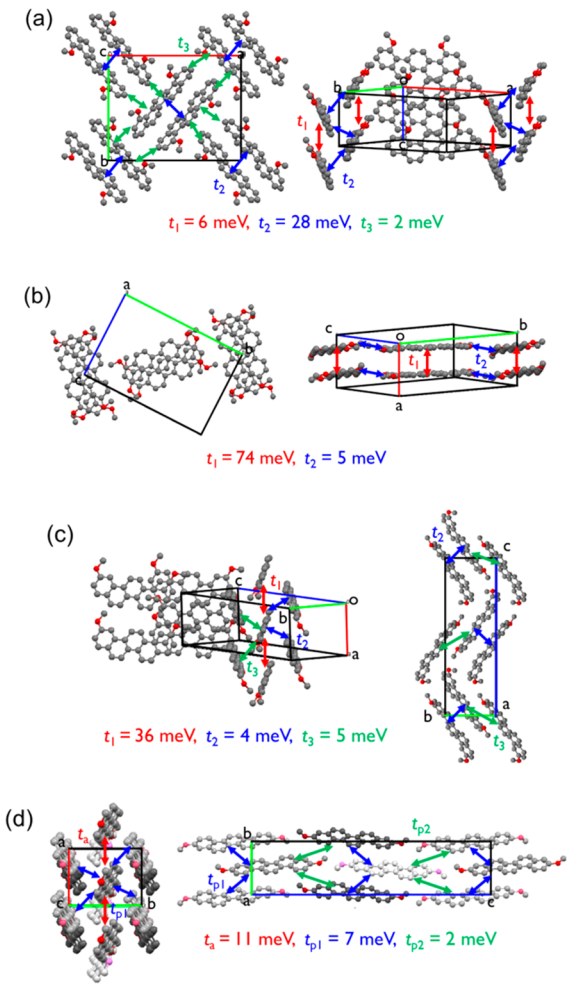

Figure 6. Packing structures and calculated intermolecular transfer integrals (*t*s) between the HOMOs of methoxy picenes using the ADF package (PW91/TZP): (a) **4a**; (b) **4b**; (c) **4c**; (d) **4e**.

The single-crystal structures of methoxy picenes **4a**−**c**,**e** are quite different from that of nonsubstituted picene.[20] These crystal structures strongly depend on the substitution position and the number of methoxy groups. From MO calculations, an intermolecular electronic coupling of **4a**−**c** depends on their packing structures because they have almost the same HOMOs as that of picene.

Compound **4b** was found to crystallize in the monoclinic space group $P2_1/n$, which is similar to that of picene. In the crystal lattice, four methoxy groups are in a conformation that extends in the same aromatic plane, but the directions of methoxy groups between the 2,11- and 4,9-positions are different. The packing structure of **4b** can thus be described as a one-dimensional (1D) $\pi-\pi$ stacking motif. Each molecule slipped along the *bc* plane and stacked in the opposite direction. In addition, each layer exists orthogonal to its neighbor. This might be explained by the steric effect of four bulky methoxy groups and their unsymmetrical structure. The transfer integrals in the stacks (i.e., along the crystallographic *a* axis direction), designated as t_1, have a large value (74 meV). However, this anisotropic 1D π-stacked structure typically limits effective carrier transport due to its discontinuous structure.[21] This suggests that the crystal structure of **4b** is probably unsuitable for a high-performance OFET.

In contrast, dimethoxypicenes **4a**,**c** crystallize in the orthorhombic space groups $Pna2_1$ and $P2_12_12_1$, respectively. Both packing structures are similar, and they partially form the herringbone packing motif. In **4a**, one dimer arranged in a herringbone manner is oriented perpendicularly with respect to another dimer plane. The transfer integrals in the *c* axis direction (t_1) and *ab* plane (t_2, face-to-edge interaction) are 6 and 28 meV, respectively, which are rather small; in particular, t_1 is significantly lower than that of nonsubstituted picene (68 meV; Figure S2, Supporting Information). This is probably because of the distorted molecular structure of **4a**, which prevents effective intermolecular interaction. Thus, the crystals of **4a** might be less effective for carrier transport in OFET devices. In comparison with **4a**, the packing structure of **4c** is a layer by layer structure with a herringbone arrangement, but it is a different structure in comparison to a typical layer-by-layer structure, as seen in that of a representative thienoacene.[21] The molecules of each layer are tilted in the opposite direction and have mutually orthogonally oriented structures. Compound **4c** exhibited relatively large transfer integrals only in the crystallographic *a* axis direction (t_1 = 36 meV), whereas the values for the other segments (t_2 = 4 meV and t_3 = 5 meV) are significantly smaller than those of picene (56 and 63 meV, respectively; Figure S2). Compound **4c** has a structure with slippage in the molecular long axis direction by about half of the length of a molecule to avoid steric hindrance of two methoxy groups. Therefore, intermolecular orbital overlaps in the crystallographic *bc* plane in **4c** are small, resulting in small transfer integrals.

Finally, **4e** crystallizes in the orthorhombic space group $P2_12_12_1$, which is the same as that of **4c**. **4e** has the smallest changes from picene among the four methoxy picenes. From the molecular arrangements projected in the *c* axis direction, the crystal structure of **4e** appears to have a typical layer-by-layer structure with a herringbone packing motif. However, molecule **4e** in the crystal slipped along the molecular long axis direction by about half the length of a molecule. This unique structure is similar to that of 3,10-dimethyldinaphtho[2,3-*b*:2′,3′-*f*]thieno[3,2-*b*]thiophene (3,10-DMDNTT) recently reported by Takimiya and co-workers.[22] The crystal structure of 3,10-DMDNTT can be described as a "3D-herringbone" packing arrangement that retains large intermolecular overlaps in the *a* axis direction (67 meV) and has relatively large overlaps (9 meV) in the *bc* plane. Its thin film acted as a superior semiconductor channel in FETs with a mobility of up to 0.8 $cm^2\ V^{-1}\ s^{-1}$. However, the transfer integral along the *a* axis direction (t_a) in the crystal of **4e** was found to be 11 meV, whereas the values for the other segments t_{p1} and t_{p2} were 7 and 2 meV, respectively. According to the picene crystal structure, there is slight displacement in the molecular long axis. Thus, the structure of **4e** with large slippage reduces its electronic coupling between adjacent molecules (i.e., t_{p1} and t_{p2}). In addition, one possible reason for these low transfer integrals along the *a* axis direction may be attributable to their HOMO density distribution; the HOMO coefficients in **4e** reside densely on the C═C bonds perpendicular to the molecular long axis direction. In fact, as can be visualized from models shown in Figure S3 (Supporting Information), the HOMO distribution of **4e** offers less effective electronic coupling in the

dx.doi.org/10.1021/jo500543h | J. Org. Chem. 2014, 79, 4973−4983

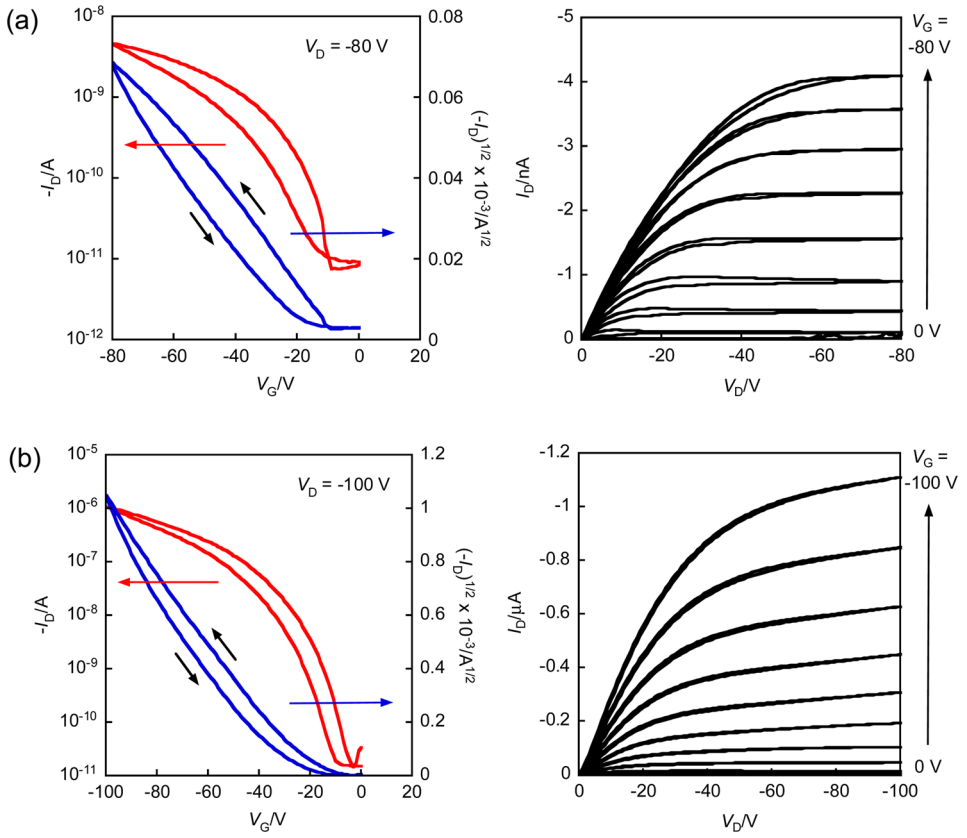

Figure 7. Transfer (left) and output (right) curves of OFETs using (a) **4c** (L = 200 μm) and (b) **4e** (L = 100 μm).

Table 3. FET Characteristics of 4c,e-Based OFET Devices Fabricated on SiO_2 Gate Dielectric (W = 500 μm)

compd	sample	L, μm	μ_h, cm^2 V^{-1} s^{-1}	V_{th}, V	$I_{on/off}$	S, V decade^{-1}
4c	1	50	5.8×10^{-5}	−3	1.1×10^3	6.6
	2	50	4.5×10^{-5}	−8	9.7×10^2	7.1
	3	100	4.4×10^{-5}	−14	2.8×10^2	7.9
	4	200	4.4×10^{-5}	−22	3.1×10^2	5.7
	5	200	1.0×10^{-4}	−7	6.2×10^2	5.2
	6	300	4.2×10^{-5}	−21	1.0×10^2	8.6
	7	450	9.5×10^{-5}	−25	1.5×10^2	6.7
	8	450	3.4×10^{-4}	−6	1.5×10^2	6.3
	av		$1(1) \times 10^{-4}$	−13(9)	$5(4) \times 10^2$	7(1)
4e	1	50	2.5×10^{-3}	−69	9.3×10^4	4.5
	2	100	1.1×10^{-2}	−31	7.5×10^4	5.0
	3	200	1.7×10^{-2}	−43	4.9×10^4	3.8
	4	200	3.0×10^{-2}	−58	5.3×10^4	5.6
	5	200	6.2×10^{-3}	−28	1.9×10^4	6.1
	6	285	1.4×10^{-2}	−52	2.0×10^4	4.2
	7	350	1.4×10^{-2}	−40	6.7×10^3	10.5
	8	450	2.1×10^{-2}	−36	3.0×10^4	3.2
	9	450	1.2×10^{-2}	−48	1.3×10^4	2.4
	10	600	1.2×10^{-2}	−48	1.4×10^4	2.6
	av		$1.4(8) \times 10^{-2}$	−45(12)	$4(3) \times 10^4$	5(2)

stacked direction than picene because **4e** has a more discontinuous HOMO distribution. We concluded that it was for this reason that low transfer integrals along the a axis direction were observed in **4e**.

OFET Characteristics and Structure−Property Relationship of 4c,e. From a structural and theoretical point of view, from among the four methoxy picenes whose structures were analyzed, **4c,e** have the potential to be OFET materials. Thus, we fabricated and characterized OFET devices using thermal evaporated thin films of **4c,e** with a device having a bottom-gate, top-contact configuration. The obtained transfer and output curves are shown in Figure 7, and extracted parameters as a function of channel length (L) from the saturation regime including the field-effect hole mobilities (μ_h), threshold voltages (V_{th}), on−off ratios ($I_{on/off}$), and subthreshold slopes (S) are summarized in Table 3. **4c**- and **4e**-based

dx.doi.org/10.1021/jo500543h | J. Org. Chem. 2014, 79, 4973−4983

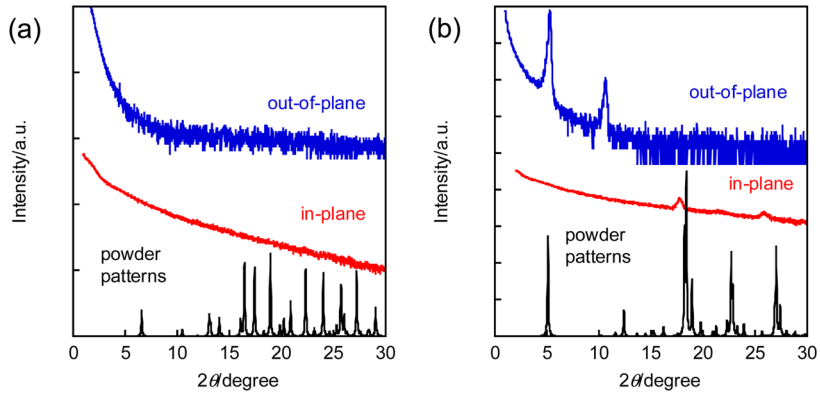

Figure 8. XRD and simulated powder patterns of (a) **4c** and (b) **4e** on an Si/SiO_2 substrate.

OFET devices both showed typical p-channel FET characteristics, and remarkable channel-length dependence was not observed. Owing to the HOMO energy levels of **4c**,**e** being higher than that of picene, smaller threshold voltages (V_{th}) for both **4c**- and **4e**-based devices were observed. However, the extracted average hole mobilities of **4c**- and **4e**-based devices were 9.6×10^{-5} and 1.4×10^{-2} cm^2 V^{-1} s^{-1}, respectively, which are 2 and 4 orders of magnitude lower, respectively, than that of picene-based OFET.[4] Considering the small t values of **4c**,**e**, the present low OFET characteristics are consistent. However, the field-effect mobility of **4c** is significantly lower than that of **4e**, though **4c** has t values larger than those of **4e**, a finding which we find rather puzzling.

In order to answer this question, we first investigated the molecular orientation in thin film by out-of-plane and in-plane XRD measurements (Figure 8). In a thin film of **4c**, no diffraction pattern was observed, indicating that it is almost amorphous on an Si/SiO_2 substrate. One possible explanation of this low crystalline nature may be its weak intermolecular interaction owing to its unsymmetrical structure. This amorphous nature of a thin film of **4c** makes it unsuitable as an efficient carrier transport in OFETs: i.e., it would result in low hole mobility. From these results, we found that the introduction of methoxy groups onto the 2,11-positions in the picene core led to large structural changes and less effective intermolecular overlaps. In contrast, defined diffraction peaks in both out-of-plane and in-plane XRD were observed in a thin film of **4e** on an Si/SiO_2 substrate. A comparison of the XRD patterns with the simulated powder patterns from the bulk single crystal clearly shows that the crystal structures of a thin film and solid state of **4e** are quite different. We found that the 3D herringbone structure of **4e** is a metastable state. Two identical diffraction peaks at 2θ = 5.28 and 10.62° were observed in the out-of-plane XRD. The calculated d spacing is 16.7 Å, which is almost the same as the molecular length (17.4 Å) of **4e** as evidenced from its single-crystal structure. This result suggests that **4e** forms a typical layer-by-layer structure in its thin film similar to the parent picene, which resembles the case of 2,9-dimethyldinaphtho[2,3-*b*:2′,3′-*f*]thieno[3,2-*b*]-thiophene (2,9-DMDNTT) reported by Takimiya and co-workers.[22] Although **4e** has a crystal structure similar to that of picene in thin films, it seems to have less effective intermolecular overlaps due to the more discontinuous HOMO distribution as seen from theoretical calculations, resulting in lower carrier mobility. However, **4e** showed the smallest structural changes in the packing structure and higher carrier mobility than that of **4c**, indicating that the introduction of methoxy groups onto the 3,10-positions (i.e., substitution in the long molecular axis direction) is the most effective approach for the development of high-performance semiconducting materials.

■ CONCLUSION

Five picenes bearing two or four methoxy groups at different positions have been selectively synthesized via the palladium-catalyzed Suzuki−Miyaura coupling or Wittig reaction and subsequent intramolecular double cyclization via C−H bond functionalizations. From the physicochemical properties and MO calculations of methoxy picenes, the positions and the numbers of methoxy groups significantly affected their electronic properties. Methoxy groups introduced onto the picene framework in the 1,12-, 2,11-, and 4,9-positions had a direct effect on their electronic structures, but the HOMO changes to another geometrical arrangement as a result of introducing the methoxy group onto the 3,10-positions. The single-crystal structure analyses of four methoxy picenes revealed that their structures are quite different from that of picene and are also influenced by the positions and the number of methoxy groups. The crystal structures were dramatically changed from a fully anisotropic 1D π-stacked structure to a unique 3D herringbone structure. From the calculations of transfer integrals on the basis of their single-crystal structures, it is evident that their intermolecular electronic coupling depends on their packing structures and/or HOMO distribution. The preliminary results of OFET with **4c**,**e** showed average hole mobilities of 9.6×10^{-5} and 1.4×10^{-2} cm^2 V^{-1} s^{-1}, respectively, which are 2 and 4 orders of magnitude lower, respectively, than that of picene due to less effective intermolecular overlaps. However, **4e** showed the smallest structural changes in the packing structure and carrier mobility higher than that of **4c**, indicating that the introduction of methoxy groups onto the 3,10-positions may be an effective approach for the future development of high-performance semiconducting materials. Such a structure−property relationship will provide us with an important clue to the design of picene-based high-performance materials in organic electronic devices. Furthermore, an understanding of the crystal structures of the four methoxy picenes examined in this study serves as motivation to design new types of picene derivatives having crystal structures that allow high-performance OFETs to be realized.

dx.doi.org/10.1021/jo500543h | J. Org. Chem. 2014, 79, 4973−4983

EXPERIMENTAL SECTION

General Experimental Methods. All of the reactions were carried out under an Ar atmosphere using standard Schlenk techniques. Glassware was dried in an oven (130 °C) and heated under reduced pressure prior to use. The ^{1}H and ^{13}C{^{1}H} NMR spectra were recorded on 300 MHz spectrometers. High-resolution mass spectra (HRMS) were obtained by fast atom bombardment (FAB) using a double-focusing magnetic sector mass spectrometer.

Solvents employed as eluents and for all other routine operations, as well as the anhydrous solvents and all reagents used, were purchased from commercial suppliers and employed without any further purification. The stereodefined (*Z*)-alkenylboronates **1a**−**d**[23] and 1,4-dichloro-2,3-diiodobenzene (**2**)[24] were prepared in accordance with the references.

Synthesis of 1,4-Dichloro-2,3-bis[(1*Z*)-2-(2-methoxyphenyl)-ethenyl]benzene (3d). To a stirred solution of **1d** (780 mg, 3 mmol) were added PEPPIS-IPr (67.9 mg 0.1 mmol, 10 mol %) and 1,4-dichloro-2,3-diiodobenzene (**2**; 398.8 mg, 1 mmol) in toluene (10 mL) and an aqueous solution of KOH (3 M) at room temperature. The reaction mixture was stirred at 110 °C for 12 h and then quenched with 1 M HCl. The organic layers extracted with diethyl ether (3 × 10 mL) were washed with brine and dried over $MgSO_4$. The subsequent filtration, evaporation of the solvent, and purification by silica gel column chromatography using ethyl acetate/hexane (1/5) as the eluents yielded **3d** (210 mg, 0.51 mmol, 51%) as a yellow oil. FT-IR (neat, cm^{-1}): 3007 (m), 2957 (m), 2836 (m), 1607 (s), 1512 (s), 1439 (m), 1304 (s), 1254 (s), 1177 (s), 1128 (m), 1034 (s), 839 (s), 754 (m), 507 (m). ^{1}H NMR showed a complex mixture of various stereoisomers. MS (EI, *m*/*z* (relative intensity)): 410 (M$^+$, 5), 304 (5), 302 (6), 289 (4), 227 (11), 189 (3), 131 (3), 122 (10), 121 (100), 77 (3). HRMS (EI): calcd for $C_{24}H_{20}Cl_2O_2$ 410.0840, found 410.0806.

1,4-Dichloro-2,3-bis[(1Z)-2-(3-methoxyphenyl)ethenyl]benzene (3a). Yellow oil. Yield: 67%. FT-IR (neat, cm^{-1}): 2938 (w), 1597 (s), 1578 (s), 1489 (s), 1435 (s), 1260 (s), 1153 (m), 1042 (s), 860 (w), 795 (s), 689 (m). ^{1}H NMR ($CDCl_3$, 300 MHz, room temperature): δ 3.60 (s, 6H), 6.10 (d, *J* = 12 Hz, 2H), 6.49 (d, *J* = 3.9 Hz, 3H), 6.55 (t, *J* = 6.6 Hz, 3H), 6.68−6.75 (m, 2H), 7.05−7.10 (m, 2H), 7.31 (s, 2H). ^{13}C{^{1}H} NMR ($CDCl_3$, 75 MHz, room temperature): δ 54.9, 112.9, 113.6, 119.3, 124.0, 125.6, 128.7, 129.1, 129.2, 132.2, 133.2, 136.0, 137.4, 138.0. MS (EI, *m*/*z* (relative intensity)): 411 (M$^+$, 5), 410 (19), 302 (16), 289 (27), 227 (79), 121 (100), 91 (14). Anal. Calcd for $C_{24}H_{20}Cl_2O_2$: C, 70.08; H, 4.90. Found: C, 69.93; H, 4.78.

1,4-Dichloro-2,3-bis[(1Z)-2-(2,4-dimethoxyphenyl)ethenyl]-benzene (3b). Yellow oil. Yield: 38%. FT-IR (neat, cm^{-1}): 2938 (w), 1608 (s), 1503 (s), 1464 (w), 1292 (s), 1290 (s), 1159, (s), 823 (w). ^{1}H NMR ($CDCl_3$, 300 MHz, room temperature): δ 3.76 (s, 6H), 3.80 (s, 6H), 6.17 (q, *J* = 8.7 Hz, 2H), 6.36 (s, 2H), 6.57 (q, *J* = 7.5 Hz, 2H), 6.78 (d, *J* = 12 Hz, 2H), 7.23 (s, 2H), 7.29 (s, 2H). ^{13}C{^{1}H} NMR ($CDCl_3$, 75 MHz, room temperature): δ 55.0, 55.4, 98.1, 104.1, 119.0, 123.5, 128.5, 128.9, 131.9, 137.9, 157.9, 160.3. MS (EI, *m*/*z* (relative intensity)): 471 (M$^+$, 7), 470 (26), 332 (12), 151 (100), 121 (16). HRMS (EI): calcd for $C_{26}H_{24}Cl_2O_4$ 470.1052, found 470.1043.

1,4-Dichloro-2,3-bis[(1Z)-2-(4-methoxyphenyl)ethenyl]benzene (3c). Yellow oil. Yield: 59%. FT-IR (neat, cm^{-1}): 3007 (m), 2955 (m), 2835 (m), 2355 (m), 1606 (s), 1512 (s), 1303 (m), 1251 (s), 1177 (m), 1034 (m), 839 (s), 754 (m), 505 (m). ^{1}H NMR showed a complex mixture of various stereoisomers. MS (EI, *m*/*z* (relative intensity)): 410 (M$^+$, 5), 304 (4), 302 (6), 289 (4), 227 (12), 189 (3), 131 (2), 126 (4), 122 (9), 121 (100), 113 (2), 77 (3). HRMS (FAB): calcd for $C_{24}H_{20}Cl_2O_2$ 410.0840, found 410.0849.

General Procedure for Synthesis of Picene Derivatives via the Pd-Catalyzed Intramolecular Annulation. Synthesis of 4d. A 20 mL Schlenk tube equipped with a magnetic stirring bar was charged with PCy_3 (11.5 mg, 0.04 mmol, 20 mol %), $PdCl_2(NCPh)_2$ (7.6 mg, 0.02 mmol,10 mol %), and DMA (1 mL) under an argon atmosphere. After the reaction mixture was stirred for 10 min, Cs_2CO_3 (130 mg, 0.4 mmol, 2.0 equiv), PivOH (8.3 mg, 0.08 mmol, 40 mol %), and substrate **3d** (70.2 mg, 0.2 mmol, 1 equiv) were added at room temperature. The tube was placed in a preheated hot box at 150 °C for 24 h. The reaction mixture was cooled to room temperature, quenched with 1 M HCl (3 mL), and extracted with chloroform (3 × 10 mL). The combined organic extracts were washed thoroughly with water and dried over anhydrous magnesium sulfate, filtered, and concentrated in vacuo. The crude residue was then purified by chromatography and HPLC to afford the product **4d** (28 mg, 42% yield) as a white solid. Mp: >300 °C. FT-IR (neat, cm^{-1}): 3003 (m), 2959 (m), 2936 (m), 2907 (m), 1607 (s), 1589 (s), 1508 (m), 1456 (s), 1416 (s), 1261 (s), 1254 (s), 1043 (s), 775 (s), 731 (m), 527 (s). ^{1}H NMR ($CDCl_3$, 600 MHz, room temperature): δ 4.08 (s, 6H), 7.04 (d, *J* = 7.8 Hz, 2H), 7.64 (t, 2H), 8.42 (d, *J* = 8.4 Hz, 2H), 8.48 (d, *J* = 9.6 Hz, 2H), 8.79 (d, *J* = 9.6 Hz, 2H), 8.89 (s, 2 H). ^{13}C{^{1}H} NMR was not observed due to the poor solubility. MS could not be obtained due to poor solubility. HRMS (EI): calcd for $C_{24}H_{18}O_2$ 338.1307, found 338.1290.

1,12-Dimethoxypicene (4a). White solid. Isolated yield: 24%. Mp: >300 °C. FT-IR (KBr, cm^{-1}): 2930 (w), 1522 (m), 1450 (s), 1427 (s), 1269 (s), 1238 (s), 1140 (s), 1059 (s), 841 (s), 820 (s), 748 (s), 704 (w). ^{1}H NMR ($CDCl_3$, 600 MHz, room temperature): δ 4.21 (s, 6H), 7.21 (q, *J* = 12 Hz, 2H), 7.58−7.64 (m, 4H), 7.96 (d, *J* = 9.6 Hz, 2H), 8.83 (d, *J* = 9.0 Hz, 2H), 9.92 (s, 2H). ^{13}C{^{1}H} NMR ($CDCl_3$, 150 MHz, room temperature): δ 55.9, 108.2, 121.1, 121.4, 122.5, 126.5, 126.6, 127.1, 128.5, 128.8, 134.3, 158.9. MS could not be detected because of the high boiling point. Anal. Calcd for $C_{24}H_{18}O_2$: C, 85.18; H, 5.36. Found: C, 85.52; H, 5.16.

2,4,9,11-Tetramethoxypicene (4b). White solid. Isolated yield: 31%. Mp: >300 °C. FT-IR (KBr, cm^{-1}): 2999 (w), 1618 (s), 1454 (m), 1416 (m), 1383 (m), 1261 (s), 1148 (s), 1047 (s), 808 (m), 644 (w). ^{1}H NMR ($CDCl_3$, 600 MHz, room temperature): δ 4.06 (s, 6H), 4.08 (s, 6H), 6.70 (d, *J* = 2.4 Hz, 2H), 7.73 (d, *J* = 1.8 Hz, 2H), 8.37 (d, *J* = 9.6 Hz, 2H), 8.64 (d, *J* = 9.0 Hz, 2H), 8.74 (s, 2H). ^{13}C{^{1}H} NMR ($CDCl_3$, 150 MHz, room temperature): δ 55.7, 56.0, 95.5, 97.9, 118.9, 119.2, 121.1, 121.6, 127.9, 129.8, 132.6, 157.3, 159.3. HRMS (EI): calcd for $C_{26}H_{22}O_4$ 398.1518, found 398.1502.

2,11-Dimethoxypicene (4c). White solid. Isolated yield: 10%. Mp: >300 °C. FT-IR (neat, cm^{-1}): 3005 (w), 2930 (w), 2832 (w), 1607 (m), 1452 (m), 1433 (m), 1211 (s), 1172 (m), 1047 (m), 1030 (m), 842 (m), 824 (s), 787 (s), 525 (m). ^{1}H NMR ($CDCl_3$, 600 MHz, room temperature): δ 4.08 (s, 6H), 7.32 (d, *J* = 1.6 Hz, 1H), 7.33 (d, *J* = 1.6 Hz, 1H), 7.92 (d, *J* = 5.6 Hz, 2H), 7.95 (d, *J* = 6.0 Hz, 2H), 8.18 (d, *J* = 1.6 Hz, 2H), 8.63 (d, *J* = 6.0 Hz, 2H), 8.81 (s, 2H). ^{13}C{^{1}H} NMR ($CDCl_3$, 150 MHz, room temperature): δ 55.5, 103.9, 117.2, 119.4, 121.4, 126.8, 127.0, 128.0, 129.1, 129.9, 131.8, 158.5. MS (EI, *m*/*z* (relative intensity)): 338 (M$^+$, 92), 323 (31), 296 (18), 295 (70), 281 (23), 280 (100), 252 (21), 250 (19), 140 (21), 126 (45), 125 (24), 113 (13). Anal. Calcd for $C_{24}H_{18}O_2$: C, 85.18, H, 5.36. Found: C, 84.92, H, 5.12.

Synthesis of 1-Bromo-2-(bromomethyl)-4-methoxybenzene (6).[25] 2-Bromo-5-methoxytoluene (**5**; 5.0 g, 24.0 mmol), *N*-bromosuccinimide (5.1 g, 28.8 mmol), and AIBN (0.1 g, 0.5 mmol, 2 mol %) were suspended in benzene (100 mL). The reaction mixture was heated to reflux for 1 h and then cooled to room temperature. The resulting mixture was filtered, and the filtrate was diluted with diethyl ether (75 mL) and washed with water (2 × 100 mL) and brine (1 × 50 mL). The organic layers were dried over $MgSO_4$ and concentrated. The crude solid was purified by silica gel column chromatography using ethyl acetate/hexane (1/10) to afford **6** (5.5 g, 21 mmol, 86%) as a white solid.

Synthesis of (2-Bromo-5-methoxybenzyl)triphenylphosphonium Bromide (7).[26] To a solution of triphenylphosphine (1.18 g, 4.5 mmol) in toluene was added 2-bromo-5-methoxybenzyl bromide (**6**; 1.25 g, 4.5 mmol). The solution was heated to reflux for 3 h and then cooled to room temperature. Subsequent filtration gave the Wittig reagent **7** (2.39 g, 20 mmol, 98%).

Synthesis of 2,2′-[1,2-Phenylenedi(1*Z*)-2,1-ethenediyl]bis(4-bromo)anisole (9) via a Wittig Reaction. To a solution of phosphonium salt **7** (2.39 g, 4.4 mmol) in THF/H_2O (10/1) was added ^{t}BuOK (740 mg, 6.6 mmol) at 0 °C. After 10 min, a solution of *o*-phthaldehyde (**8**; 134 mg, 1.0 mmol) in THF was added dropwise over 10 min. The reaction mixture was stirred at room temperature for 8 h and then quenched with water. After extraction with ethyl acetate

dx.doi.org/10.1021/jo500543h | J. Org. Chem. 2014, 79, 4973−4983

(3 × 10 mL), the organic layers were washed with brine and dried over $MgSO_4$. The solvents were removed under vacuum to give the crude product, which was purified by silica gel column chromatography using ethyl acetate/hexane (1/5) to give **9** (258 mg, 0.52 mmol, 52%) as a yellow oil. FT-IR (neat, cm^{-1}): 3055 (m), 3011 (s), 2965 (s), 2936 (s), 2836 (s), 1591 (s), 1287 (s), 1236 (s), 1175 (s), 1055 (m), 1017 (s), 962 (m), 802 (s), 600 (s). ^1H NMR ($CDCl_3$, 600 MHz, room temperature): δ 3.45 (s, 2H), 6.47 (d, J = 2.8 Hz, 2H), 6.56−6.59 (m, 2H), 6.65−6.77 (m, 4H), 7.00−7.12 (m, 4H), 7.41 (d, J = 8.8 Hz, 2H). $^{13}C\{^1H\}$ NMR ($CDCl_3$, 150 MHz, room temperature): δ 55.1, 114.6, 115.1, 115.7, 127.1, 129.5, 130.1, 130.5, 133.1, 135.5, 137.9, 158.1. MS could not be obtained because of the high molecular weight. Anal. Calcd for $C_{24}H_{20}Br_2O_2$: C, 57.63; H, 4.03. Found: C, 57.48, H, 3.78.

Synthesis of 3,10-Dimethoxypicene (4e) via the Pd-Catalyzed Intramolecular Annulation. In a 20 mL Schlenk tube equipped with a magnetic stirring bar were placed PCy_3 (11.5 mg, 0.04 mmol, 20 mol %), $PdCl_2(NCPh)_2$ (7.6 mg, 0.02 mmol, 10 mol %), and DMA (1 mL) under an argon atmosphere. After the mixture was stirred for 10 min, Cs_2CO_3 (130 mg, 0.4 mmol), PivOH (8.3 mg, 0.08 mmol, 40 mol %), and **9** (100 mg, 0.2 mmol) were added at room temperature. Then, the solution was heated to 150 °C, maintained at this temperature for 24 h, and then quenched with 1 M HCl. Subsequent filtration and washing with water gave a solid, which was isolated by silica gel column chromatography using $CHCl_3$ to afford **4e** in 10% yield (6.8 mg, 0.02 mmol) as a white solid. Mp: >300 °C. FT-IR (neat, cm^{-1}): 2955 (m), 2930 (m), 1732 (m), 1622 (s), 1603 (s), 1526 (m), 1468 (s), 1456 (s), 1435 (s), 1362 (m), 1253 (s), 1177 (s), 1020 (s), 858 (s), 810 (s), 799 (s), 750 (m). ^1H NMR ($CDCl_3$, 600 MHz, room temperature): δ 4.01 (s, 6H), 7.35 (s, 2H), 7.37 (d, J = 7.8 Hz, 2H), 7.94 (d, J = 9.3 Hz, 2H), 8.74 (d, J = 9.0 Hz, 2H), 8.83 (s, 2H). $^{13}C\{^1H\}$ NMR was not observed due to poor solubility. MS (EI, m/z (relative intensity)): 338 (M^+, 100), 295 (32), 252 (34), 250 (12), 207 (13), 131 (16), 130 (10), 126 (15), 125 (18), 113 (10). HRMS (EI): calcd for $C_{24}H_{18}O_2$ 338.1307, found 338.1286.

X-ray Structural Analyses. CCDC-976699 (**4b**), -976700 (**4c**), and -976701 (**4e**) contain supplementary crystallographic data for this paper. These data can be obtained free of charge from The Cambridge Crystallographic Data Centre via www.ccdc.cam.ac.uk/data_request/cif., by e-mailing data_request@ccdc.cam.ac.uk, or by contacting The Cambridge Crystallographic Data Centre, 12, Union Road, Cambridge CB2 1EZ, U.K. (fax (+44) 1223-336-033).

Instrumentation and Theoretical Calculations. A Pt electrode (surface area A = 0.071 cm^2, BAS), an Ag/Ag^+ electrode (Ag wire in 0.01 M $AgNO_3$/0.1 M TBAP/CH_2Cl_2), and a Pt-wire electrode were used as the working, reference, and counter electrodes, respectively. All of the potentials were calibrated with the standard ferrocene/ferrocenium redox couple (measured under identical conditions). Geometry optimizations and normal-mode calculations were performed at the B3LYP/6-31G(d) level using the Gaussian 09, Revision A.02, program package. Reorganization energies in the hole-transport system were also calculated using the same program package at the same level as the prescribed procedures.[14] Calculations of intermolecular transfer integrals were performed with the PW91 functional and Slater-type triple-ζ plus polarization (TZP) basis sets using the ADF (Amsterdam Density Functional) package. Out-of-plane and in-plane X-ray diffraction patterns of **4c**,**e** thin films deposited on hexamethyldisilazane (HMDS) treated Si/SiO_2 substrates were recorded using an X-ray diffractometer (RIGAKU Smart Lab-Pro) with a Cu Kα source (λ = 1.541 Å).

Device Fabrication and Characterization. Top-contact, bottom-gate FET devices were fabricated with thin films of **4c**,**e** formed by thermal evaporation. An SiO_2 (400 nm) insulator was used as the gate dielectric. The SiO_2 surface was treated with hexamethyldisilazane (HMDS). Au source/drain electrodes of 50 nm thickness were deposited on the **4c**,**e** thin films. 2,3,5,6-Tetrafluoro-7,7,8,8-tetracyanoquinodimethane (F4-TCNQ) of 3 nm thickness was inserted between the **4c**,**e** thin films and source/drain electrodes to decrease the contact resistance. The capacitance (C_i) was 8.35 nF cm^{-2} for HMDS-treated SiO_2. All measurements were performed at 295 K. Field-effect mobilities were calculated in the saturation regime of the I_D using the equation

$$I_D = (WC_i/2L)\mu(V_G - V_{th})^2$$

where C_i is the capacitance of the dielectric layer. I_D is the source-drain current, and V_D, V_G, and V_{th} are the source/drain, gate, and threshold voltages, respectively.

■ ASSOCIATED CONTENT

Supporting Information

Tables, figures, and CIF files giving experimental procedures, characterization data for all compounds, X-ray data for **4b**,**c**,**e**, details on MO calculations, Cartesian coordinates of calculated structures, and transfer integrals of the parent picene. This material is available free of charge via the Internet at http://pubs.acs.org.

■ AUTHOR INFORMATION

Corresponding Author

*E-mail for Y.N.: ynishiha@okayama-u.ac.jp.

Notes

The authors declare no competing financial interest.

■ ACKNOWLEDGMENTS

This work was partially supported by the MEXT program for promoting the enhancement of research universities. The authors gratefully thank Dr. Masayuki Iwasaki (Okayama University) for HRMS measurements, Profs. Koichi Mitsudo and Seiji Suga (Okayama University) for calculation of transfer integrals with ADF and CV measurements, Ms. Megumi Kosaka and Mr. Motonari Kobayashi (Department of Instrumental Analysis, Advanced Science Research Center, Okayama University) for the measurements of elemental analyses, and the SC-NMR Laboratory of Okayama University for NMR measurements.

■ REFERENCES

(1) (a) Forrest, S. R.; Thompson, M. E. *Chem. Rev.* **2007**, *107*, 923. (b) Wu, J.; Pisula, W.; Müllen, K. *Chem. Rev.* **2007**, *107*, 718. (c) Koch, N. *ChemPhysChem* **2007**, *8*, 1438. (d) Pron, A.; Gawrys, P.; Zagorska, M.; Djuradoa, D.; Demadrille, R. *Chem. Soc. Rev.* **2010**, *39*, 2577.

(2) (a) Kelley, T. W.; Muyres, D. V.; Baude, P. F.; Smith, T. P.; Jones, T. D. *Mater. Res. Soc. Symp. Proc.* **2003**, *771*, 169. (b) Ruiz, R.; Choudhary, D.; Nickel, B.; Toccoli, T.; Chang, K.-C.; Mayer, A. C.; Clancy, P.; Blakely, J. M.; Headrick, R. L.; Iannotta, S.; Malliaras, G. G. *Chem. Mater.* **2004**, *16*, 4497. (c) Katz, H. E. *Chem. Mater.* **2004**, *16*, 4748. (d) Anthony, J. E. *Chem. Rev.* **2006**, *106*, 5028. (e) Anthony, J. E. *Angew. Chem., Int. Ed.* **2008**, *47*, 452. (f) Hasegawa, T.; Takeya, J. *Sci. Technol. Adv. Mater.* **2009**, *10*, 024314.

(3) (a) Klauk, H.; Zschieschang, U.; Weitz, R. T.; Meng, H.; Sun, F.; Nunes, G.; Keys, D. E.; Fincher, C. R.; Xiang, Z. *Adv. Mater.* **2007**, *19*, 3882. (b) Maliakal, A.; Raghavachari, K.; Katz, H.; Chandross, E.; Siegrist, T. *Chem. Mater.* **2004**, *16*, 4980. (c) Coppo, P.; Yeates, S. G. *Adv. Mater.* **2005**, *17*, 3001.

(4) (a) Okamoto, H.; Kawasaki, N.; Kaji, Y.; Kubozono, Y.; Fujiwara, A.; Yamaji, M. *J. Am. Chem. Soc.* **2008**, *130*, 10470. (b) Kawasaki, N.; Kubozono, Y.; Okamoto, H.; Fujiwara, A.; Yamaji, M. *Appl. Phys. Lett.* **2009**, *94*, 043310. (c) Wang, Y.; Motta, S. D.; Negri, F.; Friedlein, R. *J. Am. Chem. Soc.* **2011**, *133*, 10054.

(5) Mitsuhashi, R.; Suzuki, Y.; Yamanari, Y.; Mitamura, H.; Kambe, T.; Ikeda, N.; Okamoto, H.; Fujiwara, A.; Yamaji, M.; Kawasaki, N.; Maniwa, Y.; Kubozono, Y. *Nature* **2010**, *464*, 76.

(6) Review: Kubozono, Y.; Mitamura, H.; Lee, X.; He, X.; Yamanari, Y.; Takahashi, Y.; Suzuki, Y.; Kaji, Y.; Eguchi, R.; Akaike, K.; Kambe,

T.; Okamoto, H.; Fujiwara, A.; Kato, T.; Kosugi, T.; Aoki, H. *Phys. Chem. Chem. Phys.* **2011**, *13*, 16476.
(7) Chang, N. H.; Chen, X. C.; Nonobe, H.; Okuda, Y.; Mori, H.; Nakajima, K.; Nishihara, Y. *Org. Lett.* **2013**, *15*, 3558.
(8) For reviews, see: (a) Echavareen, A. M.; Gómez-Lor, B.; González, J. J.; Frutos, Ó. D. *Synlett* **2003**, 585. (b) Alberico, D.; Scott, M. E.; Lautens, M. *Chem. Rev.* **2007**, *107*, 174. (c) Lyons, T. W.; Sanford, M. S. *Chem. Rev.* **2010**, *110*, 1147.
(9) For selected examples, see: (a) Wang, L.; Shevlin, P. B. *Org. Lett.* **2000**, *2*, 3703. (b) Marcinow, Z.; Sygula, A.; Ellern, A.; Rabideau, P. W. *Org. Lett.* **2001**, *3*, 3527. (c) Campeau, L. C.; Parisien, M.; Jean, A.; Fagnou, K. *J. Am. Chen. Soc.* **2006**, *128*, 581. (d) Chang, H. I.; Huang, H. T.; Huang, C. H.; Kuo, M. Y.; Wu, Y. T. *Chem. Commun.* **2010**, *46*, 7241. (e) Tsuji, H.; Ueda, Y.; Ilies, L.; Nakamura, E. *J. Am. Chem. Soc.* **2010**, *132*, 11854. (f) Peng, J. S.; Chen, T. H.; Chen, C. X.; Li, B. *J. Org. Chem.* **2011**, *76*, 9507.
(10) The Wittig reactions were carried out according to the literature procedures; for an example see: Dunne, E. C.; Coyne, É. J.; Crowley, P. B.; Gilheany, D. G. *Tetrahedron Lett.* **2002**, *43*, 2449.
(11) Fanetti, S.; Citroni, M.; Bini, R.; Malavasi, L.; Artioli, G. A.; Postorino, P. *J. Chem. Phys.* **2012**, *137*, 224506.
(12) Frisch, M. J.; Trucks, G. W.; Schlegel, H. B.; Scuseria, G. E.; Robb, M. A.; Cheeseman, J. R.; Scalmani, G.; Barone, V.; Mennucci, B.; Petersson, G. A.; Nakatsuji, H.; Caricato, M.; Li, X.; Hratchian, H. P.; Izmaylov, A. F.; Bloino, J.; Zheng, G.; Sonnenberg, J. L.; Hada, M.; Ehara, M.; Toyota, K.; Fukuda, R.; Hasegawa, J.; Ishida, M.; Nakajima, T.; Honda, Y.; Kitao, O.; Nakai, H.; Vreven, T.; Montgomery, J. A., Jr.; Peralta, J. E.; Ogliaro, F.; Bearpark, M.; Heyd, J. J.; Brothers, E.; Kudin, K. N.; Staroverov, V. N.; Kobayashi, R.; Normand, J.; Raghavachari, K.; Rendell, A.; Burant, J. C.; Iyengar, S. S.; Tomasi, J.; Cossi, M.; Rega, N.; Millam, N. J.; Klene, M.; Knox, J. E.; Cross, J. B.; Bakken, V.; Adamo, C.; Jaramillo, J.; Gomperts, R.; Stratmann, R. E.; Yazyev, O.; Austin, A. J.; Cammi, R.; Pomelli, C.; Ochterski, J. W.; Martin, R. L.; Morokuma, K.; Zakrzewski, V. G.; Voth, G. A.; Salvador, P.; Dannenberg, J. J.; Dapprich, S.; Daniels, A. D.; Farkas, Ö.; Foresman, J. B.; Ortiz, J. V.; Cioslowski, J.; Fox, D. J. *Gaussian 09, Revision A.02*, Gaussian, Inc., Wallingford, CT, 2009.
(13) Osaka, I.; Shinamura, S.; Abe, T.; Takimiya, K. *J. Mater. Chem. C* **2013**, *1*, 1297.
(14) (a) Brédas, J. L.; Beljonne, D.; Coropceanu, V.; Cornil, J. *Chem. Rev.* **2004**, *104*, 4971. (b) Sakanoue, K.; Motoda, M.; Sugimoto, M.; Sakaki, S. *J. Phys. Chem. A* **1999**, *103*, 5551.
(15) (a) Salman, S.; Delgado, M. C. R.; Coropceanu, V.; Brédas, J. L. *Chem. Mater.* **2009**, *21*, 3593. (b) Saranya, G.; Navamani, K.; Senthikumar, K. *Chem. Phys.* **2014**, *433*, 48.
(16) Torii, S. *Electroorganic syntheses: methods and applications*; VCH: Weinheim, Germany, 1985; Part 1 (Oxidations).
(17) See the Supporting Information.
(18) *ADF 2013.01: powerful DFT code for modeling molecules*; Scientific Computing and Modeling, Amsterdam; http://www.scm.com/ADF/.
(19) (a) Senthilkumar, K.; Grozema, F. C.; Bickelhaupt, F. M.; Siebbeles, L. D. A. *J. Chem. Phys.* **2003**, *119*, 9808. (b) Prins, P.; Senthilkumar, K.; Grozema, F. C.; Jonkheijm, P.; Schenning, A. P. H. J.; Meijer, E. W.; Siebbeles, L. D. A. *J. Phys. Chem. B* **2005**, *109*, 18267.
(20) De, A.; Ghosh, R.; Roychowdhury, S.; Roychowdhury, P. *Acta Crystallogr., Sect. C* **1985**, *C41*, 907.
(21) Takimiya, K.; Shinamura, S.; Osaka, I.; Miyazaki, E. *Adv. Mater.* **2011**, *23*, 4347.
(22) Kang, M. J.; Yamamoto, T.; Shinamura, S.; Miyazaki, E.; Takimiya, K. *Chem. Sci.* **2010**, *1*, 179.
(23) (a) Stewart, S. K.; Whiting, A. *J. Organomet. Chem.* **1994**, *482*, 293. (b) Kiesewetter, E. T.; O'Brien, R. V.; Yu, E. C.; Meek, S. J.; Schrock, R. R.; Hoveyda, A. H. *J. Am. Soc. Chem.* **2013**, *135*, 6026.
(24) Nakayama, J.; Sakai, A.; Hoshino, M. *J. Org. Chem.* **1984**, *49*, 5084.
(25) Mello, J. V.; Finney, N. S. *J. Am. Chem. Soc.* **2005**, *127*, 10124.
(26) Kamikawa, K.; Takemoto, I.; Takemoto, S.; Matsuzaka, H. *J. Org. Chem.* **2007**, *72*, 7406.